Mathematical Modelling and Numerical Analysis
Modélisation Mathématique et Analyse Numérique

Will be set by the publisher

STICK-SLIP TRANSITION CAPTURING BY USING AN ADAPTIVE FINITE ELEMENT METHOD

N. Roquet and P. Saramito[1]

Abstract. The numerical modeling of the fully developed Poiseuille flow of a Newtonian fluid in a square section with slip yield boundary condition at the wall is presented. The stick regions in outer corners and the slip region in the center of the pipe faces are exhibited. Numerical computations cover the complete range of the dimensionless number describing the slip yield effect, from a full slip to a full stick flow regime. The resolution of variational inequalities describing the flow is based on the augmented Lagrangian method and a finite element method. The localization of the stick-slip transition points is approximated by an anisotropic auto-adaptive mesh procedure. The singular behavior of the solution at the neighborhood of the stick-slip transition point is investigated.

Résumé. Nous présentons la résolution numérique de l'écoulement de Poiseuille établi d'un fluide newtonien dans un tuyau de section carrée avec une condition au bord de glissement à seuil. Nous montrons l'apparition de zones d'adhérence près des coins sortants et de zones de glissement au milieu des faces du tuyau. Les calculs numériques recouvrent complètement le domaine du nombre sans dimension décrivant l'effet de seuil pour le glissement, d'un glissement total à une adhésion totale. La résolution des inéquations variationnelles dérivant l'écoulement utilise la méthode du Lagrangien augmenté et une méthode d'éléments finis. La localisation du point de transition adhérence-glissement est approchée par une méthode d'éléments finis auto-adaptative. Nous explorons aussi la singularité de la solution au voisinage du point de transition adhérence-glissement.

1991 Mathematics Subject Classification. 65N30, 65N50, 90C46, 65N22, 65Z05.

January 19, 2004.

1. Introduction

One of the difficult problems in numerical fluid computation is to describe slip at the boundary, especially when the slip is submitted to a yield value. In that case, the boundary condition is not linear. This situation occurs in many cases of practical interest: geophysical, food or petroleum fluid flows. In some cases, the material is not a Newtonian fluid: it would be viscoplastic or viscoelastic. Furthermore, the determination of the regions where the material slips or sticks are of practical interest, e.g. for earth cracks or for extrusion processes.

The fully developed flow in a tube with a square cross-section (see Fig. 1) contains the main features of such flows. In *stick regions*, located near the outward corners of the section, the shear stresses are low and the velocity vanishes at the boundary (see Fig. 2). Conversely, in *slip regions*, located at the center of the pipe

Keywords and phrases: Slip boundary condition, stick-slip problem, variational inequalities, adaptive mesh, computational fluid mechanics

[1] LMC-IMAG, B.P. 53, 38041 Grenoble cedex 9, France. Corresponding author: Pierre.Saramito@imag.fr

faces, the shear stresses are higher and the fluid slips. Tube transition points between these two regions are called the stick-slip transition points.

To our knowledge, there are no numerical computations related to this subject. Our numerical strategy combines the augmented Lagrangian method that takes rigorously into account the slip yield stress constitutive equation, and the auto-adaptive mesh procedure for the capture of the stick-slip transition points.

The section two presents the slip boundary problem of the flow along a prismatic tube. The numerical method is presented in the third section. This is an adaptation to the slip yield condition of a numerical strategy presented in [12–14] in the context of a Bingham fluid. The analogy between the slip yield condition and the Bingham yield stress constitutive equation allows us to extend the algorithms to the present case. The fourth section presents results on a square cross-section. Three flow regimes are exhibited and the evolution of the stick-slip transition point is carefully studied. The local behavior of the slip velocity at the neighborhood of the stick-slip transition point is analyzed.

2. Problem statement

2.1. Constitutive equation and conservation laws

Let σ_{tot} denotes the total Cauchy stress tensor:

$$\sigma_{\text{tot}} = -p.I + \sigma,$$

where σ denote its deviatoric part, and p the pressure. The slip boundary condition reads :

$$\mathbf{u_t} = \begin{cases} -\left(1 - \frac{s_0}{|\sigma_{\boldsymbol{\nu t}}|}\right) \frac{\sigma_{\boldsymbol{\nu t}}}{c_f}, & \text{when } |\sigma_{\boldsymbol{\nu t}}| > s_0, \\ 0, & \text{otherwise,} \end{cases}$$

where $\mathbf{u}$ is the velocity field, $s_0 \geq 0$ the slip yield stress and $c_f > 0$ the friction dissipation coefficient. The notations $\mathbf{u_t}$ and $\sigma_{\boldsymbol{\nu t}}$ are defined by

$$\begin{aligned} \mathbf{u_t} &= \mathbf{u} - (\mathbf{u}.\boldsymbol{\nu})\,\boldsymbol{\nu}, \\ \sigma_{\boldsymbol{\nu t}} &= \sigma.\boldsymbol{\nu} - (\sigma_{\boldsymbol{\nu\nu}})\,\boldsymbol{\nu}, \end{aligned}$$

where $\sigma_{\boldsymbol{\nu\nu}} = (\sigma.\boldsymbol{\nu}).\boldsymbol{\nu}$ and $\boldsymbol{\nu}$ is the unit outward normal vector. For any vector field $\mathbf{v}$, the notation $|.|$ represents the vector norm $|\mathbf{v}| = (\mathbf{v}.\mathbf{v})^{1/2}$. Notice that the vector field $\sigma_{\boldsymbol{\nu t}}$ is tangent to the boundary and that $\sigma_{\boldsymbol{\nu\nu}}$ is a scalar field defined on the boundary. The slip relation can be also written as:

$$\begin{aligned} &\sigma_{\boldsymbol{\nu t}} = -c_f \mathbf{u_t} - s_0 \tfrac{\mathbf{u_t}}{|\mathbf{u_t}|}, && \text{if } |\mathbf{u_t}| \neq 0, \\ &|\sigma_{\boldsymbol{\nu t}}| \leq s_0, && \text{if } |\mathbf{u_t}| = 0. \end{aligned}$$

The boundary condition is completed by a condition expressing that the fluid does not cross the boundary:

$$\mathbf{u}.\boldsymbol{\nu} = 0.$$

Remark that for $s_0 = 0$, one obtains the classical linear slip boundary condition: the fluid slips for any non-vanishing shear stress $\sigma_{\boldsymbol{\nu t}}$. For $s_0 > 0$, boundary parts where the fluid sticks can be observed. As s_0 becomes larger, these stick regions develop. This simple law can be extended, as mentioned by Fortin *et al.* [5] or Ionescu and Vernescu [10]. In the context of solid mechanics and contact problems, Coulomb type friction has been studied by many authors. Refer e.g. to Haslinger *et al.* [8, p. 377] for the numerical analysis and to Kikuchi and Oden [11] for the finite element approximation. In this case, the slip yield stress s_0 is no more a constant, and should be replaced by a quantity s that depends upon the pressure at the boundary: $s = c_0|\sigma_{\boldsymbol{\nu\nu}}|$. Nevertheless, previous works do not study the stick-slip transition. In this paper, since our purpose is to study a new numerical algorithms for the stick-slip transition capturing, we suppose that the slip yield stress is a constant.

The conservation of momentum is:

$$\rho\left(\frac{\partial \mathbf{u}}{\partial t} + \mathbf{u}.\nabla\mathbf{u}\right) - \mathbf{div}\,\sigma + \nabla p = 0,$$

where ρ is the constant density. Since the fluid is supposed to be incompressible, the mass conservation leads to:

$$\operatorname{div}\mathbf{u} = 0.$$

In this paper, the fluid is supposed to be Newtonian:

$$\sigma = 2\eta D(\mathbf{u})$$

here $D(\mathbf{u}) = (\nabla\mathbf{u} + \nabla\mathbf{u}^T)/2$ and $\eta > 0$ is the constant viscosity.

We consider the fully developed flow in a prismatic tube (see Fig 1). Let (Oz) be the axis of the tube and (Oxy) the plane of the bounded section $\Omega \subset I\!R^2$. The pressure gradient is written as $\nabla p = (0, 0, -f)$ in Ω, where $f > 0$ is the constant applied force density.

2.2. The pipe flow problem

The velocity is written as $\mathbf{u} = (0, 0, u)$, where the third component u along the (Oz) axis depends only upon x and y, and is independent of t and z. The problem can be written as a two-dimensional one:

(P): find u defined in Ω such that

$$-\eta\Delta u = f \text{ in } \Omega, \tag{1}$$

$$u = \left\{ \begin{array}{ll} -\left(1 - \dfrac{s_0}{\left|\eta\dfrac{\partial u}{\partial n}\right|}\right)\dfrac{\eta}{c_f}\dfrac{\partial u}{\partial n}, & \text{when } \left|\eta\dfrac{\partial u}{\partial n}\right| > s_0 \\ 0, & \text{otherwise} \end{array} \right\} \text{ on } \partial\Omega, \tag{2}$$

where $\mathbf{n}$ is the unit outward normal vector on the boundary $\partial\Omega$ of the cross section Ω.

Let L be a characteristic length of the cross-section Ω, e.g. the half-length of an edge of a square section. A characteristic velocity is given by $U = L^2 f/\eta$. The slip yield dimensionless number S is defined as the ratio of the slip yield stress s_0 to a characteristic stress $\Sigma = \eta U/L = Lf$:

$$S = \frac{s_0}{Lf}. \tag{3}$$

The friction dimensionless number C_f is defined by

$$C_f = \frac{c_f U}{\Sigma} = \frac{c_f L}{\eta}. \tag{4}$$

The two dimensionless numbers S and C_f characterize the problem. The C_f coefficient is chosen equal to the unity for all numerical experiments, and the S parameter alone varies in this paper.

3. Numerical method

The augmented Lagrangian method, applied to problem (1)-(2), is briefly introduced in this paragraph. Then, the delicate problem of the choice of a finite element approximation is carefully treated.

3.1. **Augmented Lagrangian algorithm**

Let $H^1(\Omega)$ denote the classical functional Sobolev space [1] and J the convex functional defined for all $v \in H^1(\Omega)$ by

$$J(v) = \frac{\eta}{2}\int_\Omega |\nabla v|^2 \,\mathrm{d}x + c_f \int_{\partial\Omega} |\gamma v|^2 \,\mathrm{d}s + s_0 \int_{\partial\Omega} |\gamma v| \,\mathrm{d}s - \int_\Omega f v \,\mathrm{d}x$$

where $\mathrm{d}s$ is a measure on $\partial\Omega$ and γ is the trace operator from $H^1(\Omega)$ to $H^{1/2}(\partial\Omega)$, i.e. γv is the restriction $v_{|\partial\Omega}$ of v on $\partial\Omega$.

Using variational inequality methods (see e.g. Glowinski *et al.* [7]) we show that the solution u of problem (P) is characterized as the minimum of J on $H^1(\Omega)$:

$$\min_{v\in H^1(\Omega)} J(v). \tag{5}$$

Let us introduce the linear constraint

$$\xi = \gamma u \in H^{1/2}(\partial\Omega). \tag{6}$$

This constraint is handled by using a Lagrangian multiplier $\lambda \in L^2(\partial\Omega)$ that coincides with the shear stress $\boldsymbol{\sigma}.\mathbf{n}$ at the boundary. The Lagrangian $\mathcal{L}$ is defined for all $(u, \xi, \lambda) \in H^1(\Omega) \times (L^2(\partial\Omega))^2$ by

$$\begin{aligned}\mathcal{L}(u,\,\xi;\,\lambda) \;=\; & \frac{\eta}{2}\int_\Omega |\nabla u|^2 \,\mathrm{d}x - \int_\Omega f u \,\mathrm{d}x \\ & + \frac{c_f}{2}\int_{\partial\Omega} |\xi|^2 \,\mathrm{d}s + s_0 \int_{\partial\Omega} |\xi| \,\mathrm{d}s + \int_{\partial\Omega} \lambda\,(\xi - \gamma u)\,\mathrm{d}s.\end{aligned}$$

For all $a > 0$, the augmented Lagrangian

$$\mathcal{L}_a(u,\,\xi;\,\lambda) = \mathcal{L}(u,\,\xi;\,\lambda) + \frac{a}{2}\int_{\partial\Omega} (\xi - \gamma u)^2 \,\mathrm{d}s$$

is quadratic and positive-definite with respect to u. This implies that, with λ and ξ fixed, $\mathcal{L}_a$ can be minimized with respect to u on $H^1(\Omega)$, whereas this operation is in practice impossible for $a = 0$. This transformation proves to be helpful since we can solve the saddle-point problem of $\mathcal{L}_a$, that coincides with that of $\mathcal{L}$, by an appropriate algorithm proposed in [6]:

ALGORITHM (Uzawa)

initialization: $n = 0$

Let λ^0 and ξ^0 be arbitrarily chosen in $L^2(\partial\Omega)$.

loop: $n \geq 0$

- **step 1**: Suppose λ^n and ξ^n are known and find $u^{n+1} \in H^1(\Omega)$ such that

$$-\eta\Delta u^{n+1} = f \qquad \text{in } \Omega, \tag{7}$$

$$\eta\frac{\partial u^{n+1}}{\partial n} + a u^{n+1} = \lambda^n + a\xi^n \text{ on } \partial\Omega. \tag{8}$$

- **step 2**: compute explicitly on $\partial\Omega$:

$$\xi^{n+1} := \begin{cases} \left(1 - \dfrac{\sigma_0}{|\lambda^n + a\gamma u^{n+1}|}\right)\dfrac{\lambda^n + a\gamma u^{n+1}}{c_f + a}, & \text{if } |\lambda^n + a\gamma u^{n+1}| > \sigma_0, \\ 0, & \text{otherwise.} \end{cases} \tag{9}$$

• **step 3**: compute explicitly on $\partial\Omega$:

$$\lambda^{n+1} := \lambda^n + a(\xi^{n+1} - \gamma u^{n+1}). \tag{10}$$

end loop

The advantage of this algorithm is that it transforms the global non-differentiable problem (5) into a family of completely standard problems (7)-(8) and a local explicit computation (9), coordinated via the Lagrange multiplier in (10). The sequence (u^n, ξ^n, λ^n) converges for all $a > 0$ to (u, ξ, λ) where $u \in H^1(\Omega)$ is the solution to (5) and $\xi = u_{|\partial\Omega}$ and $\lambda = \eta \frac{\partial u}{\partial n}$ on $\partial\Omega$.

3.2. Finite element approximation

Let A and B be the two bilinear forms defined by:

$$\begin{aligned} A(u,\, \xi;\, v,\, \zeta) &= \eta \int_\Omega \nabla u.\nabla v \,\mathrm{d}x + (c_f + a) \int_{\partial\Omega} \gamma u\, \gamma v \,\mathrm{d}s + a \int_{\partial\Omega} (\xi\zeta - \gamma u\, \zeta - \xi\, \gamma v) \,\mathrm{d}s, \\ B(v,\, \zeta;\, \mu) &= \int_{\partial\Omega} \mu\, (\zeta - \gamma v) \,\mathrm{d}s. \end{aligned}$$

The saddle point of $\mathcal{L}_a$ is characterized as the solution of a problem expressed by the following variational inequalities:

(VI): *find* $(u,\, \xi;\, \lambda) \in H^1(\Omega) \times (L^2(\partial\Omega))^2$ *such that*:

$$\begin{array}{rcccccl} s_0 \displaystyle\int_{\partial\Omega} (|\zeta| - |\xi|) \,\mathrm{d}s & + & A(u,\, \xi;\, v,\, \zeta - \xi) & + & B(v,\, \zeta - \xi;\, \lambda) & \geq & \displaystyle\int_\Omega f\, v \,\mathrm{d}x, \\ & & B(u,\, \xi;\, \mu). & & & = & 0 \end{array}$$

for all $(v,\, \zeta;\, \mu) \in H^1(\Omega) \times (L^2(\partial\Omega))^2$.

Let $V_h \subset H^1(\Omega)$, $\Xi_h \subset L^2(\partial\Omega)$, and $\Lambda_h \subset L^2(\partial\Omega)$ be some finite dimensional spaces. The finite dimensional version of the variational inequalities is simply obtained by replacing functional spaces by their finite dimensional counterparts:

$(VI)_h$: *find* $(u_h,\, \xi_h;\, \lambda_h) \in V_h \times \Xi_h \times \Lambda_h$ *such that*:

$$\begin{array}{rcccccl} \sigma_0 \displaystyle\int_{\partial\Omega} (|\zeta| - |\xi_h|) \,\mathrm{d}s & + & A(u_h,\, \xi_h;\, v,\, \zeta - \xi_h) & + & B(v,\, \zeta - \xi_h;\, \lambda_h) & \geq & \displaystyle\int_\Omega f\, v \,\mathrm{d}x, \\ & & B(u_h,\, \xi_h;\, \mu) & & & = & 0, \end{array}$$

for all $(v,\, \zeta;\, \mu) \in V_h \times \Xi_h \times \Lambda_h$.

The choice $\Xi_h = \Lambda_h$ leads to $\xi_h = R_h \gamma u_h$ where R_h denotes the projection from $L^2(\partial\Omega)$ on Λ_h, defined for all $\varphi \in L^2(\Omega)$ by:

$$R_h\varphi \in \Lambda_h \text{ and } \int_{\partial\Omega} R_h\varphi\, \zeta \,\mathrm{d}s = \int_{\partial\Omega} \varphi\, \zeta \,\mathrm{d}s, \quad \forall \zeta \in \Lambda_h.$$

For $s_0 = 0$, the problem reduces to a linear one that fits the theory of mixed finite elements (see e.g. [3]). See also [4] for the use of the properties of R_h in the context of stabilized mixed finite element approximation. The case $s_0 = 0$ together with the choice $\Xi_h = \Lambda_h$ leads to $\lambda_h = -c_f R_h \gamma u_h$ and the problem reduces to the following linear elliptic one:

$(Q)_h$ *find* $u_h \in V_h$ *such that*

$$\eta \int_\Omega \nabla u_h . \nabla v \, \mathrm{d}x + c_f \int_{\partial\Omega} R_h \gamma u_h \, R_h \gamma v \, \mathrm{d}s + a \int_{\partial\Omega} (I - R_h)\gamma u_h \, (I - R_h)\gamma v \, \mathrm{d}s = \int_\Omega f \, v \, \mathrm{d}x, \quad \forall v \in V_h .$$

When $R_h \neq I$ i.e. $\Lambda_h \neq \gamma V_h$, the discrete solution u_h depends upon the numerical parameter $a > 0$ of the augmented Lagrangian method. This property is not desirable. A necessary and sufficient condition for the solution u_h to be independent of the parameter a is therefore $\Lambda_h = \gamma V_h$.

Let $\mathcal{T}_h$ be a finite element mesh made up of triangles and let $\partial\mathcal{T}_h$ denote the corresponding mesh of the boundary $\partial\Omega$, consisting in segments. We introduce the space V_h of continuous piecewise polynomials of order $k \geq 1$, relative to $\mathcal{T}_h$:

$$V_h = \{v \in H^1(\Omega);\ v_{|K} \in P_k,\ \forall K \in \mathcal{T}_h\}.$$

Thus, $\Lambda_h = \Xi_h = \gamma V_h$ is the set of continuous piecewise polynomial functions defined on the mesh boundary $\partial\mathcal{T}_h$

$$\Xi_h = \Lambda_h = \{\mu \in L^2(\partial\Omega) \cap C^0(\partial\Omega);\ \mu_{|S} \in P_k,\ \forall S \in \partial\mathcal{T}_h\}.$$

Numerical experiments presented in this paper use piecewise linear polynomials, i.e. $k = 1$.

3.3. **Mesh adaptation**

The mesh adaptation procedure has already been described in [13,14] for a Bingham fluid flow problem, and thus, only the main steps are presented in this paragraph.

Following Vallet [17], a way to adapt the mesh to the computation of a *governed field* is to equi-distribute its error of interpolation, i.e. to make it constant over all triangles and in all directions. Solving a problem using a mesh adaptation is an iterative process, which involves three main steps:

1.: Starting from an initial mesh $\mathcal{T}_0$, the problem is solved using the augmented Lagrangian algorithm, yielding a solution $u^{(0)}$. to the mesh $\mathcal{T}_0$.

2.: Let $\varphi^{(0)} = |\nabla u^{(0)}|$ be the governing field. This field emphasizes regions where the solution has high derivatives, so that the mesh generator refines these regions.

3.: Starting from the governing field $\varphi^{(0)}$ on the mesh $\mathcal{T}_0$, an anisotropic adaptive mesh generator (see Borouchaki *et al.* [2], Hecht [9]) generates a totally new mesh, denoted by $\mathcal{T}_1$.

Then, $\mathcal{T}_1$ is used to solve the problem, and so on, until the solution obtained reaches an accurate localization of the stick-slip transition point. This method is based on the fact that high second derivatives of the velocity develop at the neighborhood of the stick-slip transition point, and thus the mesh generator refines this neighborhood. The singular behavior of the second derivative of the velocity at the neighborhood of the transition point will be analyzed in detail in the next section. The software is based on a finite element library released by the authors [15,16].

In order to reduce the computational cost in the square cross-section, we exploit the symmetries of the solutions with respect to the Ox, Oy and the $x = y$ axis. Thus the domain of computation reduces to a triangle (see again Fig. 2). Fig. 3 shows the mesh after 15 adaptation loops and for a slip yield number $S = 0.385$, as defined in (3). The stick-slip transition point is close to the corner $x = y = L$, and the stick region is small. Observe that the mesh adaptation process is able to catch the stick-slip transition point.

4. Numerical experiments on the square section

4.1. **Flow regimes**

Observe on Fig. 4.a the velocity profile along the boundary $u_{|\partial\Omega}(y) = u(L, y)$ for various values of S. When S increases, the stick region develops. Each profile is a decreasing curve, with a vanishing tangent at the

origin. Moreover, at each point of the boundary, the velocity is a decreasing function of S. Let us denote by $y_t(S) \in [0, L]$ the stick-slip transition point. The slip region is then defined by $[0, y_t(S)[$ and the stick region by $]y_t(S), L]$. Remark that there exists S values with empty stick region, for instance $S = 0$. Conversely, for some other values of S, slip regions are empty. Since the velocity is decreasing with S, there are three flow regimes:

1.: A *full slip regime*: the fluid slips all along the boundary. This regime is characterized by $S \leq S_L$, where $S_L \approx 0.382$ is the threshold value (S_L stands for slip).

2.: A *full stick regime*: the fluid sticks all along the boundary. This regime is characterized by $S \geq S_T$, where $S_T \approx 0.674$ is the limit value (Soa stands for stick).

3.: A *mixed stick-slip regime*: there exists a stick-slip transition point $y_t(S) \in]0, L[$. This regime is characterized by $S_L < S < S_T$.

A dichotomy algorithm has been used to obtain the approximate values of S_L and S_T.

In the full slip regime, the solution is obtained by a simple translation from the solution u_0 associated to $S = 0$:

$$u_S(x, y) = u_0(x, y) - S, \quad 0 \leq S \leq S_L.$$

Recall that the problem for $S = 0$ is a linear Poisson problem with Robin boundary conditions:

$$-\eta \Delta u_0 = f \text{ in } \Omega \quad \text{and } \eta \frac{\partial u_0}{\partial n} + c_f u_0 = 0 \text{ on } \partial\Omega.$$

In the full stick regime, the solution does not depend upon S:

$$u_S(x, y) = u_\infty(x, y), \quad S \geq S_T,$$

where u_∞ is obtained by solving a linear Poisson problem with Dirichlet boundary conditions:

$$-\eta \Delta u_\infty = f \text{ in } \Omega \quad \text{and } u_\infty = 0 \text{ on } \partial\Omega.$$

Thus, the problem reduces to the study of the mixed stick-slip regime $S_L < S < S_T$.

Then, observe on Fig. 4.b the evolution of the minimal and maximal velocity at the boundary as a function of S:

$$u_{\max}(S) = u_S(L, 0) \quad \text{and} \quad u_{\min}(S) = u_S(L, L).$$

In the mixed stick-slip regime, $u_{\max}$ is no more an affine function of S and seems to vanish at $S = S_T$ with an horizontal slope.

Observe on Fig. 5.a and 5.b the velocity profiles along symmetry axes. Again, the plots show that $u_S = u_0 - S$ for $S \geq S_L$. When S increases from S_L to S_T (Fig. 5.c and 5.d) the profiles decrease and tend to the profiles associated to $S = S_T$. For greater values of S, the velocity does not change any more.

4.2. **The neighborhood of the stick-slip point**

Fig. 6 shows the first and the second tangential derivatives of the slip velocity along the boundary. Fig. 6.a suggests that the tangential derivative $\frac{\partial u_{|\partial\Omega}}{\partial t}$ shows a vertical slope, as we can check on Fig. 6.b, where the second derivative exhibits a peak at the stick-slip transition point.

Fig. 7 plots the slip velocity along the boundary at the neighborhood of the stick-slip transition point by using a logarithmic scale. Observe the asymptotic behavior for $y \approx y_t(S)$, which seems to obey to a power law. Thus, let us look at the neighborhood of $y = y_t(S)$, $y < y_t(S)$ for

$$u_S \approx c(S) \times \{y_t(S) - y\}^{\alpha(S)}.$$

For each value of S, the values for $\alpha(S)$ and $c(S)$ are computed numerically by a non-linear least square fitting procedure. The coefficient α is provided in the table on Fig. 8 together with the stick-slip location point $y_t(S)$

for $S = 0.4$, 0.5 and 0.6. The second tangential derivative is singular at the neighborhood of the stick-slip transition point:

$$\frac{\partial^2 u_S}{\partial t^2} \approx k(S) \times \{y_t(S) - y\}^{\alpha(S)-2}.$$

Since $\alpha(S)$ increases with S, the singularity is stronger for small values of S, i.e. at the neighborhood $S \approx S_L$, $S > S_L$, as we can observe on Fig. 6.b.

Fig. 9 shows the stick-slip transition point as a function of S. The slope seems to be vertical in $S = S_T$: when S decreases and reaches the S_T values, a slip occurs and the stick-slip transition point y_t goes rapidly away from the neighborhood of $y_t = 0$: The associated stick region $[0, y_t]$ grows very fast.

5. Global maximal and mean values

Fig. 10 plots the maximal and mean velocities as a function of S. These curves are affine in the full slip regime, gradually varied in the stick-slip regime, and becomes constant for the full stick regime $S = S_T$ with an horizontal slope. Despite the appearance of the stick-slip transition point in the mixed stick-slip flow regime, the maximal and mean values depend smoothly on S.

6. Conclusion

A new numerical method for slip yield boundary conditions as been addressed in this paper. Such problems are characterized by the existence of a stick-slip transition point located on the boundary. The location of this point depends upon the parameters of the problem and is *a priori* unknown. An important result is the accurate capture of this transition point and the determination of three flow regimes.

The results of the present paper extend results [12–14] that have been developed in the context of Bingham fluids: the combination of an adaptive mesh strategy and the augmented Lagrangian method. Applied here to a square cross-section, the present numerical procedure can be applied to a tube section of any shape.

Slip yield boundary conditions is of practical interest and great importance in many geophysical and industrial applications involving complex materials. In the future, we will turn to non-Newtonian fluids problems involving slip yield boundary conditions.

References

[1] R. A. Adams. *Sobolev spaces.* Academic Press, 1975.

[2] H. Borouchaki, P. L. George, F. Hecht, P. Laug, and E. Saltel. Delaunay mesh generation governed by metric specifications. Part I: Algorithms. *Finite Elem. Anal. Des.*, 25:61–83, 1997.

[3] F. Brezzi and M. Fortin. *Mixed and Hybrid Finite Element Methods.* Springer Verlag, 1991.

[4] F. Brezzi, M. Fortin, and R. Stenberg. *Error analysis of mixed-interpolated elements for Reissner-Mindlin plates.* Research Repport n^0 780, Instituto di Analisi Numerica, Pavie, 1991.

[5] A. Fortin, D.Côté, and P.A. Tanguy. On the imposition of friction boundary conditions for the numerical simulation of Bingham fluid flows. *Comput. Meth. Applied Mech. Engrg.*, 88:97–109, 1991.

[6] M. Fortin and R. Glowinski. *Méthodes de lagrangien augmenté. Applications à la résolution numérique de problèmes aux limites.* Méthodes Mathématiques de l'Informatique, Dunod, 1982.

[7] R. Glowinski, J. L. Lions, and R. Trémolières. *Numerical analysis of variational inequalities.* North Holland, Amsterdam, 1981.

[8] J. Haslinger, I. Hlavàček, and J. Nečas. *Numerical methods for unilateral problems in solidmechanics.* Handbook of Numerical Analysis, vol. IV, P. G. Ciarlet and J. L. Lions (ed.), 1996.

[9] F. Hecht. *Bidimensional anisotropic mesh generator.* INRIA, 1997. `http://www-rocq.inra.fr/gamma/cdrom/www/bamg`.

[10] I. R. Ionescu and B. Vernescu. A numerical method for a viscoplastic problem. An application to the wire drawing. *Int. J. Engrg. Sci.*, 26:627–633, 1988.

[11] N. Kikuchi and J. T. Oden. *Contact problems in elasticity: A study of variational inequalities and finite element methods.* SIAM Studies in Applied Mathematics, 1988.

[12] Nicolas Roquet, Richard Michel, and Pierre Saramito. Errors estimate for a viscoplastic fluid by using P_k finite elements and adaptive meshes. *C. R. Acad. Sci. Paris, Série I*, 331(7):563–568, 2000.

[13] Nicolas Roquet and Pierre Saramito. An adaptive finite element method for Bingham fluid flows around a cylinder. submitted, 2001.

[14] Pierre Saramito and Nicolas Roquet. An adaptive finite element method for viscoplastic fluid flows in pipes. *Comput. Meth. Applied Mech. Engrg.*, 190:5391–5412, 2001.

[15] Pierre Saramito and Nicolas Roquet. Rheolef home page. `http://www-lmc.imag.fr/lmc-edp/Pierre.Saramito/rheolef/`, 2002.

[16] Pierre Saramito and Nicolas Roquet. Rheolef users manual. Technical report, LMC-IMAG, 2002. `http://www-lmc.imag.fr/lmc-edp/Pierre.Saramito/rheolef/usrman.ps.gz`.

[17] M. G. Vallet. *Génération de maillages anisotropes adaptés. Application à la capture de couches limites.* Rapport de Recherche n^0 1360, INRIA, 1990.

List of Figures

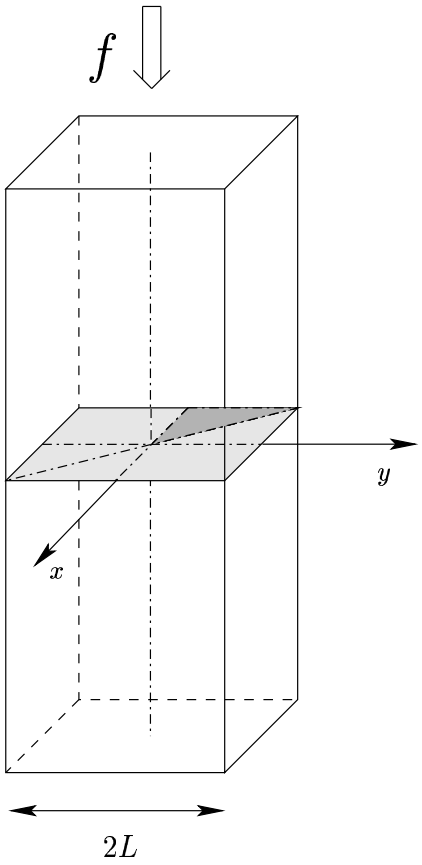

FIGURE 1. Square tube cross-section: tridimensional view

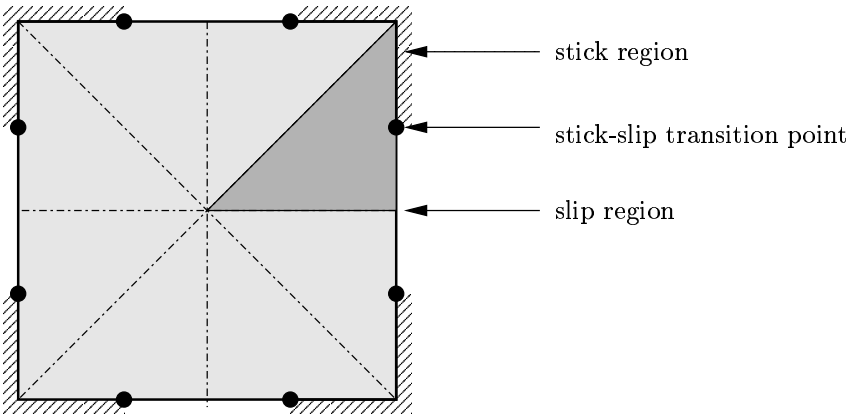

FIGURE 2. Schematic view of the cross-section.

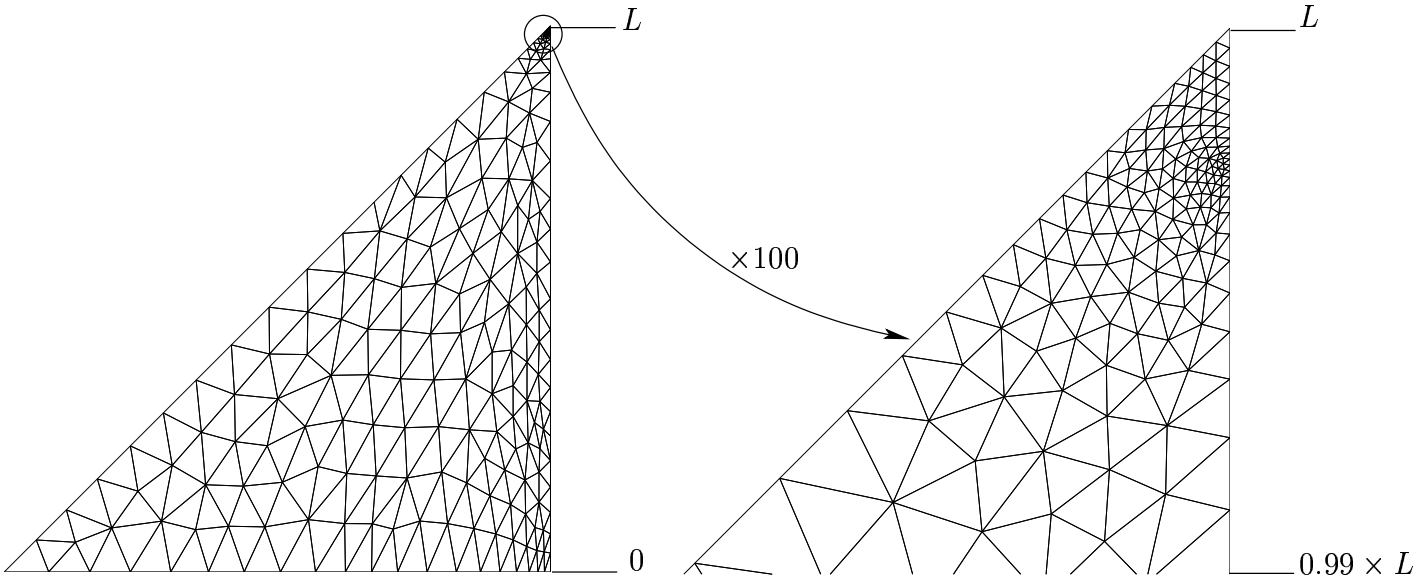

FIGURE 3. Zoom ×100 at the neighborhood of the stick-slip transition point: after 15 mesh adaptation iterations ($S = 0.385$).

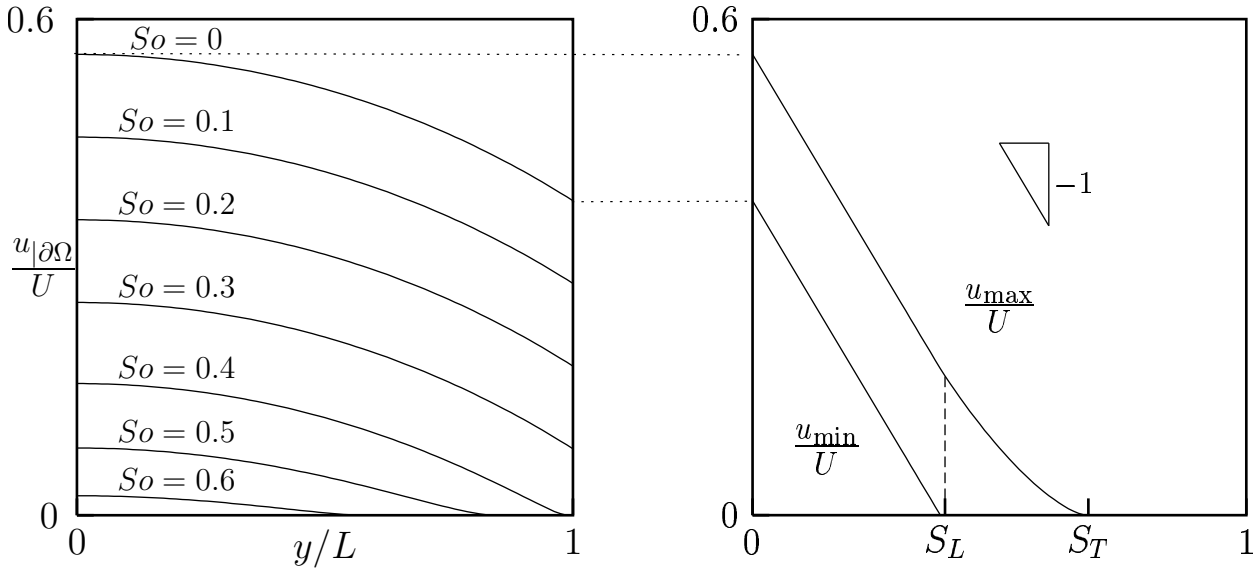

FIGURE 4. Slip velocity on the boundary: (a) for various S values ; (b) extremal slip velocities as a function of S.

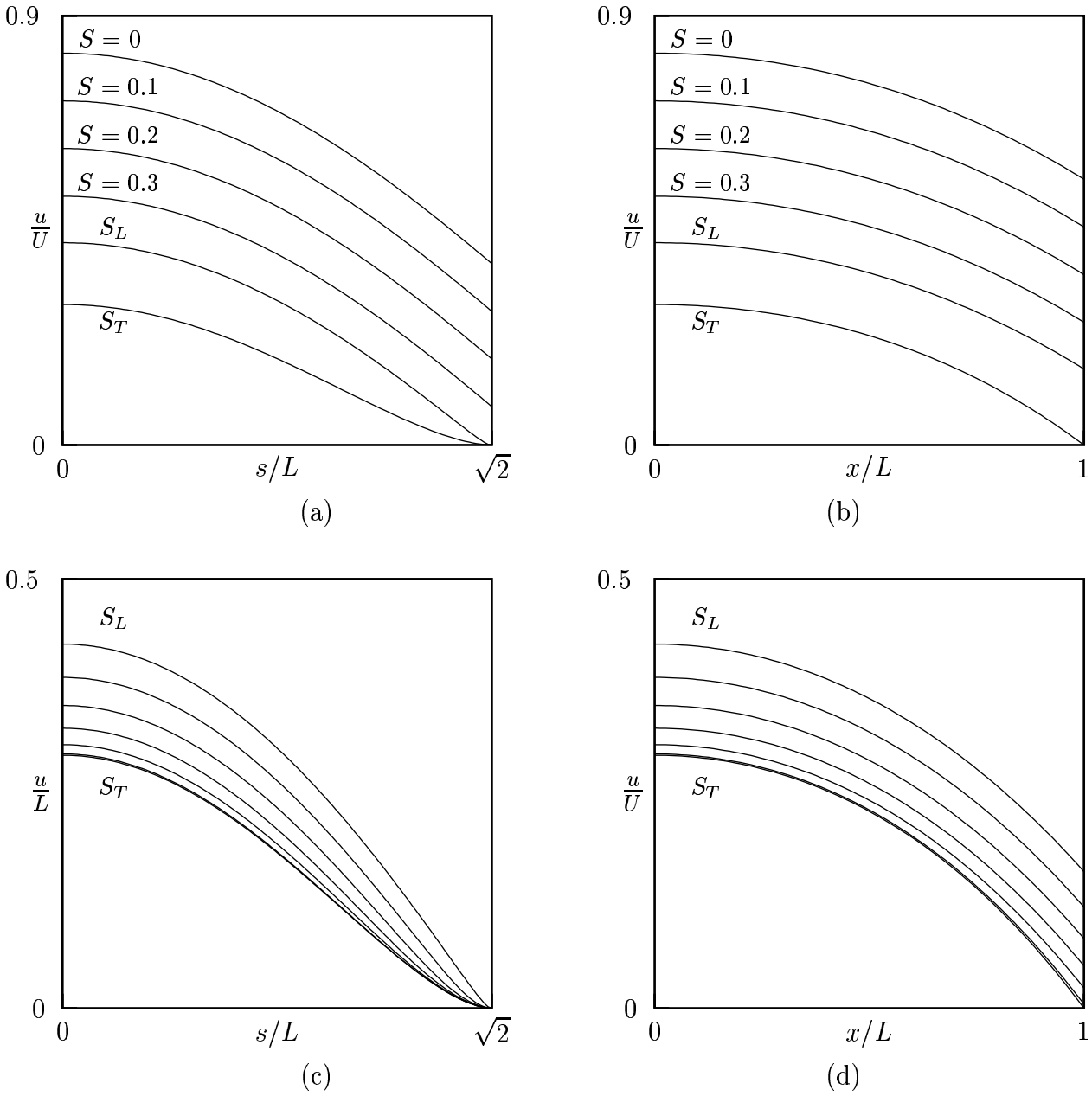

FIGURE 5. Velocity profile along the symmetry axes for various S values : (a) along the diagonal symmetry axis for $0 \leq S \leq S_T$; (b) along the horizontal symmetry axis for $0 \leq S \leq S_T$; (c) along the diagonal symmetry axis for $S_L \leq S \leq S_T$; (d) along the horizontal symmetry axis for $S_L \leq S \leq S_T$.

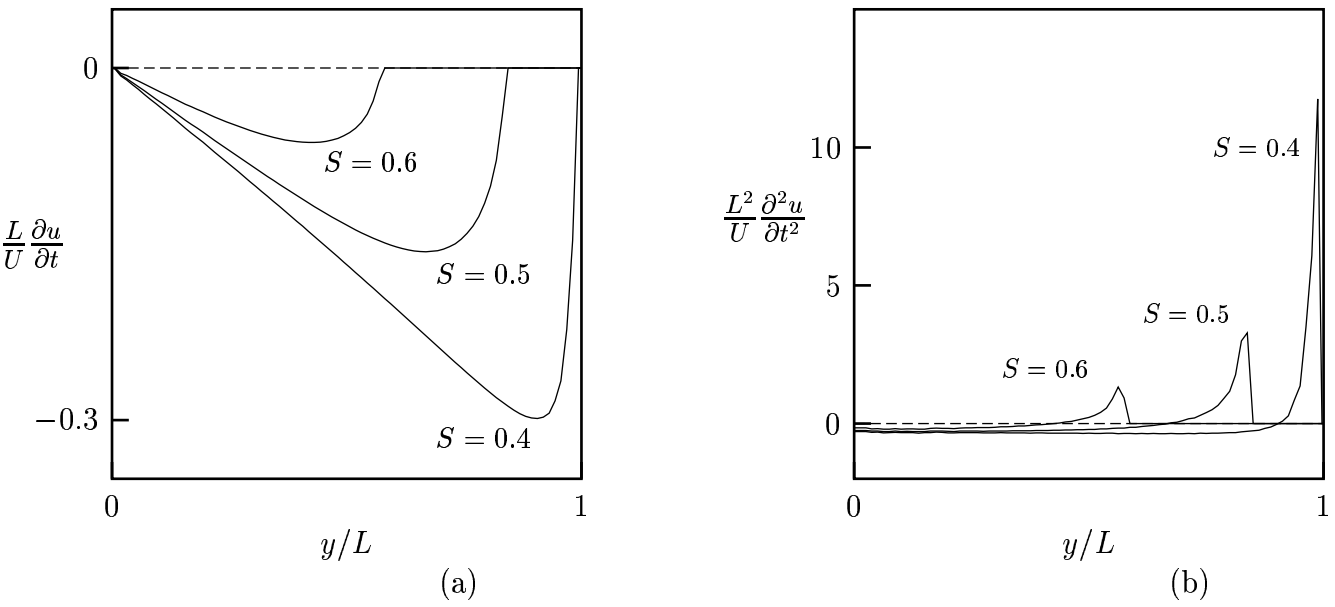

FIGURE 6. First (a) and second (b) tangential derivatives of the slip velocity along the boundary.

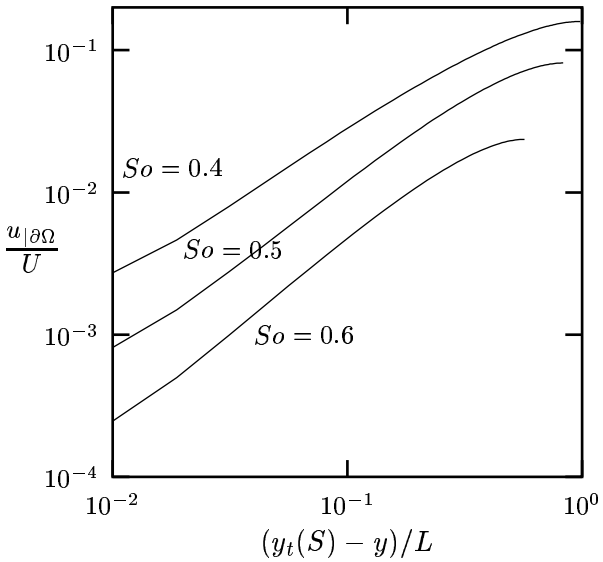

FIGURE 7. Behavior of the slip velocity at the neighborhood of the stick-slip boundary point.

S	$\alpha(S)$	$y_t(S)$
0.4	1.08	0.98
0.5	1.25	0.83
0.6	1.33	0.57

FIGURE 8. Coefficient $\alpha(S)$ at the stick-slip point transition $y_t(S)$.

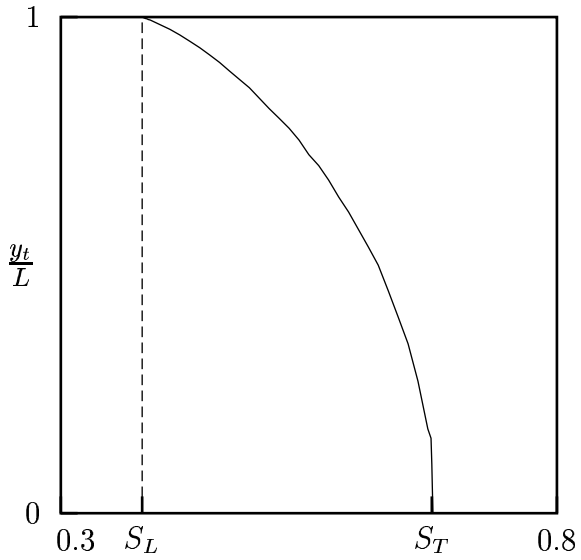

FIGURE 9. Coordinate of the stick-slip transition point $y_t(S)$ as a function of S.

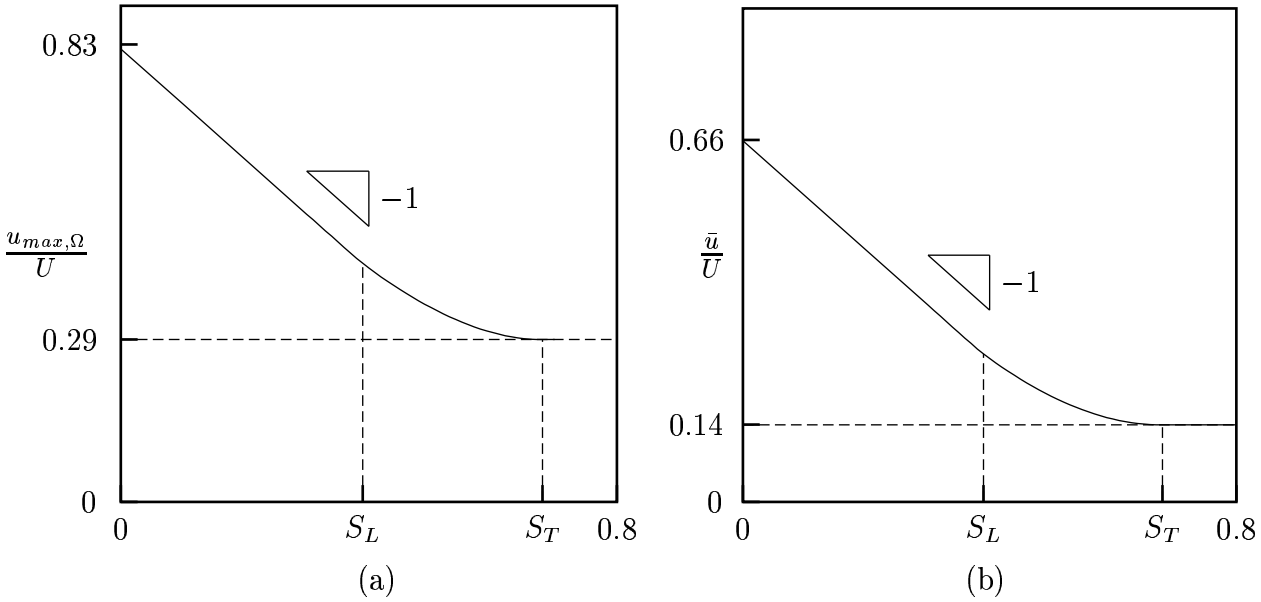

FIGURE 10. Maximal (a) and mean (b) velocities as a function of S.